

Molecular modeling and dynamic simulation of chicken Mx protein with the S631N polymorphism

Vijayakumar Gosu, Donghyun Shin, Ki-Duk Song, Jaeyoung Heo & Jae-Don Oh

To cite this article: Vijayakumar Gosu, Donghyun Shin, Ki-Duk Song, Jaeyoung Heo & Jae-Don Oh (2022) Molecular modeling and dynamic simulation of chicken Mx protein with the S631N polymorphism, Journal of Biomolecular Structure and Dynamics, 40:2, 612-621, DOI: 10.1080/07391102.2020.1819419

To link to this article: <https://doi.org/10.1080/07391102.2020.1819419>



View supplementary material [↗](#)



Published online: 22 Sep 2020.



Submit your article to this journal [↗](#)



Article views: 174



View related articles [↗](#)



View Crossmark data [↗](#)



Citing articles: 3 View citing articles [↗](#)



Molecular modeling and dynamic simulation of chicken Mx protein with the S631N polymorphism

Vijayakumar Gosu^{a#}, Donghyun Shin^{b,c#}, Ki-Duk Song^{a,b,c}, Jaeyoung Heo^d and Jae-Don Oh^a

^aDepartment of Animal Biotechnology, Jeonbuk National University, Jeonju, Republic of Korea; ^bThe Animal Molecular Genetics and Breeding Center, Jeonbuk National University, Jeonju, Republic of Korea; ^cDepartment of Agricultural Convergence Technology, Jeonbuk National University, Jeonju, Republic of Korea; ^dInternational Agricultural Development and Cooperation Center, Jeonbuk National University, Jeonju, Republic of Korea

Communicated by Ramaswamy H. Sarma

ABSTRACT

Myxovirus resistance (Mx) proteins are antiviral GTPases induced by type I interferons (IFNs). In chickens, a single Mx protein variant, S631N, has been suggested to possess antiviral activity. However, the impact of this variant on chicken Mx (chMx) protein structure and conformation has not been investigated. Hence, in this study, we applied computational methods such as molecular modeling, molecular dynamic simulation, inter domain motion and residue networks to examine the structure and dynamic behavior of wild-type and mutant chMx. At first, we built 3-dimensional structural models for both wild-type and mutant chMx proteins, which revealed that the structural organization of chMx was similar to that of human Mx proteins. Subsequently, molecular dynamics simulations revealed that angle variation around the hinge1 region led to the different stalk domain conformations between the wild-type and mutant chMx proteins. Domain motion analysis further suggested that the conformational differences in the loop region surrounded by the mutant residue may lead to an inclined stalk domain conformation in the mutant compared to the wild-type protein. In addition, we performed betweenness centrality analysis from residue interaction networks, to identify the crucial residues for intramolecular signal flow in chMx. The results of this study provided information on the differences in structure and dynamics between wild-type and mutant chMx, which may aid in understanding the structural features of the S631N mutant, that may be associated with chMx protein antiviral activity.

ARTICLE HISTORY

Received 16 April 2020
Accepted 22 August 2020

KEYWORDS

Mx protein; polymorphism; molecular dynamics simulation; essential dynamics; interdomain motion; residue networks


Introduction

Interferon (IFN)-induced immune responses play an important role in antiviral defense (Muller et al., 1994). Myxovirus resistance (Mx) proteins are type I IFN-induced, dynamin-like GTPases (Haller et al., 2007, 2015; Haller & Kochs, 2002), which restrict the replication of several RNA viruses, as well as some DNA viruses (Rothman et al., 1990). Mx genes are conserved from yeasts to vertebrates (Pavlovic & Staeheli, 1991; Staeheli, 1990). In mammals, there are two Mx protein orthologs, i.e. MxA and MxB. Despite the high sequence and structural homology of MxA and MxB, the two proteins exhibit independent mechanisms of action and appear to act against different viral families. Mouse and human MXAs mediate resistance to the influenza virus (Haller & Kochs, 2011; Zürcher et al., 1992), whereas MxB is associated with antiviral activity against human immune-deficiency viruses (Goujon et al., 2013; Kane et al., 2013; Liu et al., 2013). In contrast to mammals, in chickens and ducks, only one Mx protein has been identified. However, the antiviral activity of chicken Mx (chMx) protein remains unclear. Previous studies have reported that, despite its detectable expression, chMx

exhibits no antiviral activity (Bazzigher et al., 1993; Bernasconi et al., 1995). However, another study showed that among the single nucleotide polymorphisms (SNPs) identified in *chMx*, some are associated with Mx-mediated resistance to vesicular stomatitis virus *in vitro* (Sasaki et al., 2013). Among these variants, chMx with a substitution of serine residue to asparagine at position 631 (S631N, chMx^{S631N}) shows antiviral activity *in vitro* (Ko et al., 2004) and is associated with cytokine responses, as well as reductions in morbidity, early mortality, and viral shedding (Ewald et al., 2011). However, another study showed contradictory results for the antiviral activity of chMx (Benfield et al., 2008). The antiviral activity of chMx^{S631N} is also debatable, due to conflicting results obtained from different groups (Dillon & Runstadler, 2010; Ewald et al., 2011; Schusser et al., 2011; Wang et al., 2012). One study reported chMx^{S631N} to be associated with antiviral activity in avian influenza virus (AIV)-infected embryos and broilers (Wang et al., 2012). However, another study reported that chMx^{S631N} lacks GTPase activity and is dispensable for interferon-mediated resistance against AIV in chicken cells (Schusser et al., 2011). Therefore, since the

CONTACT Jae-Don Oh  ohsow@naver.com; Jaeyoung Heo  hyheobio@gmail.com  Jeonbuk National University, Jeonju 54896, Republic of Korea

[#]Vijayakumar Gosu and Donghyun Shin contributed equally to this work.

 Supplemental data for this article can be accessed online at <https://doi.org/10.1080/07391102.2020.1819419>.

© 2020 Informa UK Limited, trading as Taylor & Francis Group

antiviral activity of chMx is debatable, exploration of the structure and dynamics of chMx protein (chMx^{WT} and chMx^{S631N}) may help shed light on its function.

Crystal structures have been solved for human Mx protein, and these suggest that the protein contains the following three domains: a guanosine triphosphate (GTP)-binding domain, crucial for the activity due to GTP binding; three bundle signaling elements (BSEs), with several hydrophobic interactions within BSE helices; and a long stalk domain, which is important for multimerization. In all of the crystal structures of human Mx, loop 4 of the stalk domain has been found to be disordered (Chen et al., 2017; Gao et al., 2011). However, in a recent study, the cryo-EM structure of human MxB was determined, which revealed the presence of a helix as part of loop 4 in the stalk domain (Alvarez et al., 2017). Moreover, two hinge regions were also found to be present. Hinge1 is crucial for the flexibility between helix 4 of the stalk domain and BSE3, whereas hinge2 is located between the GTP-binding domain and BSE2. To date, the crystal structure of chMx protein has not been determined. Thus, it may be difficult to understand the structure-function relationship between wild-type and mutant chMx proteins. Moreover, chMx shows ~47% identity with human Mx proteins. Hence, in this study, to understand the impact of the S631N variant, in terms of structural aspects, we built three-dimensional (3D) models of wild-type (chMx^{WT}) and mutant (chMx^{S631N}) chMx proteins and subsequently, performed long-range molecular dynamics (MD) simulations, principal components (PCs) analysis, and interdomain motion analysis, to understand the structural differences between the chMx^{S631N} mutant and the wild-type chMx protein.

Materials and methods

Modeling of chMx protein

We identified several sequences with SNPs in the *chMx* gene in the UniProt database; however, we chose the core chMx protein sequence as our main focus to understand the impact of the S631N polymorphism on protein structure and to infer the structural differences between the wild-type and mutant chMx proteins. We retrieved the amino acid sequence of the chMx protein from the UniProt database (ID: Q90597). We then submitted the sequence to the BLAST server against the Protein Data Bank database. We found that the structures of human MxA and MxB were similar to the structure of the chMx protein, with ~47% identity. However, all the observed crystal structures had several missing residues, particularly in the loop regions. Therefore, we submitted the chMx protein sequence to the I-TASSER webserver (Roy et al., 2010; Yang et al., 2015), which is the most popular online tool for automated structural prediction and annotation. The template structures used by the I-TASSER server to predict the chMx protein model are presented in Table S1. We obtained 5 models from I-TASSER and based on the C-scores (an indicator of the quality of the models predicted by I-TASSER server), we selected the structural model of chMx^{WT}. Subsequently, this model was subjected to the ModRefiner server (<https://zhanglab.ccmb.med.umich.edu/>

ModRefiner/), to remove the steric bumps/clashes in the structural model (Xu & Zhang, 2011). To construct the mutant model, i.e. chMx^{S631N}, we replaced the serine at position 631 with asparagine, using Discovery Studio Visualizer (Discovery Studio 2.1; Accelrys Inc., San Diego, CA, USA). Subsequently, we performed energy minimization for both wild-type and mutant proteins using GROMACS 5.1.4. Finally, the stereochemical properties were checked using a Ramachandran plot.

Molecular dynamics simulations

The chMx protein models were further subjected to atomistic molecular dynamics simulations using GROMACS 5.1.4 (Pronk et al., 2013; Van Der Spoel et al., 2005), with an AMBER99-sb-ILDN force field (Lindorff-Larsen et al., 2010), as reported in our previous study (Gosu et al., 2019). Both native and mutant proteins were solvated with tip3p water molecules in a dodecahedron box with a periodic distance of 1.4 nm. Since the protein showed a net zero charge, we did not include ions to neutralize the system. Energy minimization was performed using the steepest gradient method with 1,000 KJ/nm. Coulomb and Van der Waals interactions were truncated at 1.0 nm. The NVT ensemble simulations were performed for 100 ps, and subsequently, 500 ps NPT simulations were performed using positional restraints. A V-rescale thermostat (Bussi et al., 2007) and a Parrinello-Rahman barostat (Parrinello & Rahman, 1981) were used to maintain the temperature at 300 K and the pressure at 1.0 bar, respectively. Finally, a production run of 200 ns was performed in the absence of positional restraints. Total 3 independent simulations were performed using different initial velocities. The 2-fs time step were used and 2 ps coordinates were saved for the analysis. The analyses of RMSD, RMSF, Rg, and angle were performed using the GROMACS analysis modules, gmx rms, gmx rmsf, gmx gyrate, and gmx angle, respectively. In addition, protein figures were prepared using PyMOL and graphs were prepared using Excel.

Principal component and free energy landscape analysis

Principal components (PCs) were assessed for the wild-type and mutant chMx proteins using the MD trajectories (Amadei et al., 1999; Gosu et al., 2019; Yamaguchi et al., 1998). The concatenated trajectory of last 100 ns from each MD trajectory was used with a time step of 10 ps coordinates for the backbone atoms of the wild-type and mutant chMx proteins. Rotational and translational movements were removed using the least squares fit method. Eigenvalues and eigenvectors were extracted using the gmx covar and gmx anaeig modules in GROMACS (van Aalten et al., 1995; Yamaguchi et al., 1998). Further, the gmx sham module was used to calculate the free energy landscape (FEL) from different structural conformations extracted for the dominant modes (PC1 and PC2). Mathematica version 12 was used to extract the FEL plot.

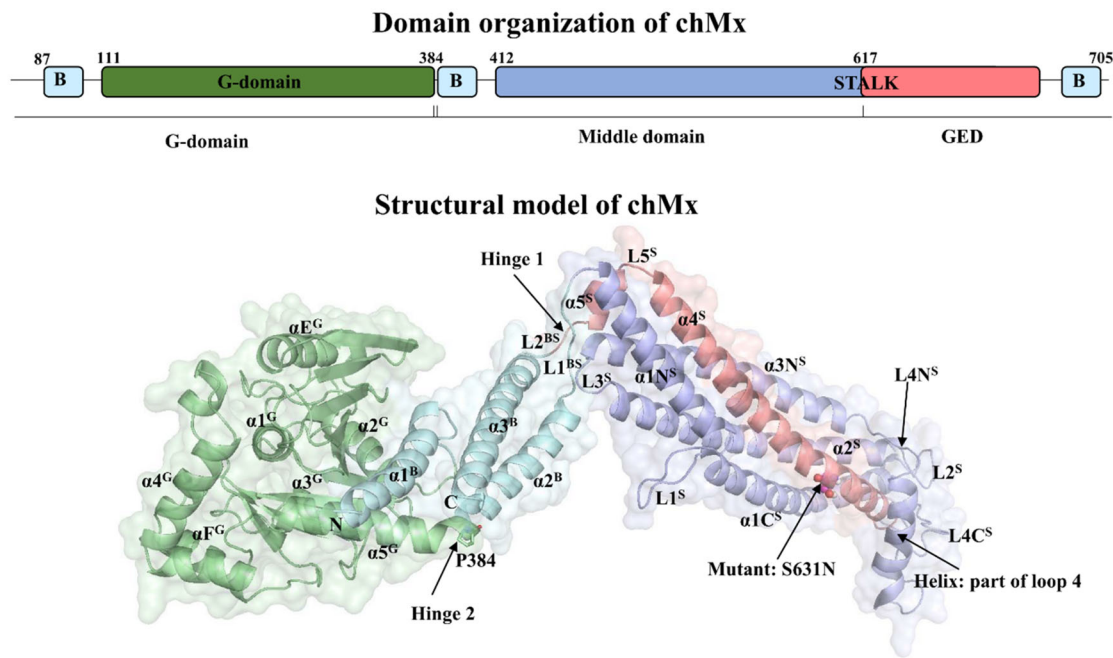


Figure 1. Domain and structural organization of the chicken Mx protein. The domain organization of the chicken Mx (chMx) protein is presented (top). The residual range of the G-domain (green), bundle signaling element (BSE, cyan), and stalk domain (light blue and pink) is shown. Overall, the domain organization consists of a G-domain, comprising BSE (first helix) and a GTP-binding domain; a middle domain, comprising a BSE (second helix) and a stalk domain (first three helices); and finally, a GTPase effector domain (GED), comprising a stalk domain (helix 4) and a BSE (third helix). The secondary structural features of chMx protein are also shown. The GTP-binding domain contains β -sheets and a helix bundle (green), the BSE contains three helices in different positions (cyan), and the stalk domain contains 4 helices (light blue and pink). The labelling of the secondary structure is based on the crystal structure of human MxA/MxB. The mutant residue is shown in the ball and stick model (magenta), and hinge 1 and hinge 2 are labeled on the structure. The helix that is a part of loop 4 of the stalk domain is also indicated. G, G-domain; B, BSE; S, stalk domain.

Interdomain motion analysis

To assess the interdomain motions for both wild-type and mutant chMx proteins, we used the DynDom program (Girdlestone & Hayward, 2016; Hayward, 1999; Hayward & Berendsen, 1998) implemented as a webserver (<http://dyndom.cmp.uea.ac.uk/dyndom/runDyndom.jsp>). We used the initial and final (representative structures from MD simulations) conformations with default parameters, such as a window length of 5 and a minimum domain size of 20. By using two different conformations of the same protein, the DynDom program identified domains based on clustering the displacement vectors and recognized the location and orientation of the hinge axes as either twist (parallel) or closure (perpendicular) axes.

Residue network analysis

Residue networks were constructed using the NAPS webserver (Chakrabarty & Parekh, 2016) for the representative structures of both the wild-type and mutant chMx proteins with a non-weighted edge and a $C\alpha$ - $C\alpha$ pair maximum threshold of 7 Å. From this analysis, we determined the betweenness centrality (C_B) values, which may be functionally important for signal transduction within the protein.

Results

Structural models of wild-type and mutant chMx proteins

We first performed multiple sequence alignment of chMx and huMxA/MxB using the T-coffee expresso webserver and Esprit 3

(sequence similarity and secondary structural annotation), which showed that huMxA/MxB proteins were $\sim 47\%$ identical to chMx protein (Figure S1A). Further, 3D structural model of wild-type chMx protein were built using the I-TASSER webserver, with several templates (Table S1), mainly using Cryo-EM structure of human MxB (PDB ID: 5UOT). Though, cryo-EM structure was solved at low resolution (4.6 Å), this structure contains less disordered region compared to the crystal structures available for human MxA/B. In particular, the loop 4 region of the STALK domain are largely disordered in the crystal structures. The RMSD between modeled and template structure (PDB ID: 5UOT) was $\sim 1\text{Å}$ (Figure S1B); to construct mutant chMx protein, we used wild-type model to replace the serine 631 with asparagine and both the models were subsequently subjected to energy minimization using the GROMACS package. Finally, the stereochemical properties were evaluated using a Ramachandran plot. The Ramachandran plot showed that 92.7% (wild-type) and 91.2% (mutant) of amino acids were in the favored region, 5.5% (wild-type) and 7.6% (mutant) were in the allowed region, and 1.8% (wild-type) and 1.2% (mutant) were in the outlier region. It is worth mentioning that when more than 90% of amino acids are in the favored region, the model is considered to be good. The structural architecture of the full-length chMx protein, which was similar to that of human MxA/MxB, showed a GTP-binding domain, three BSEs, and a stalk domain (Figure 1).

Structural dynamics of the wild-type and mutant chMx proteins

We performed three independent simulation runs with different initial velocities for both the wild-type (chMx^{WT}) and

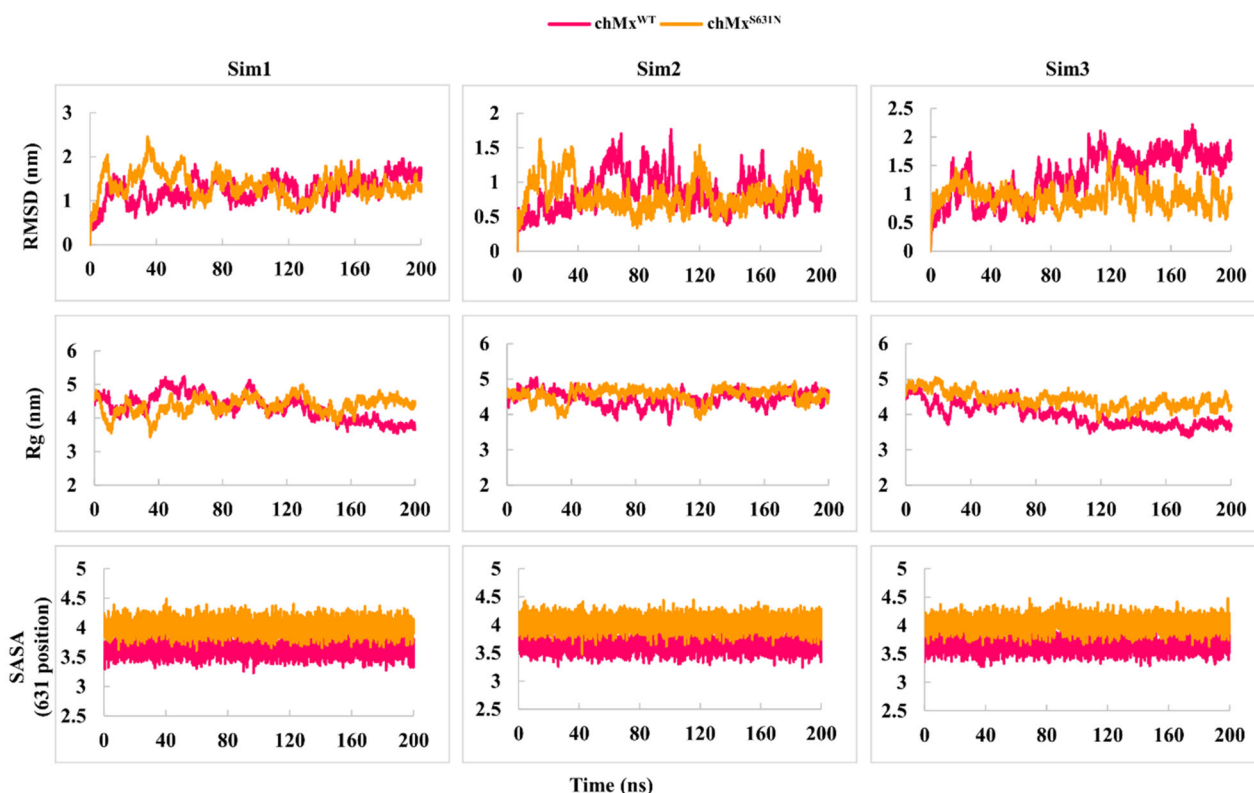


Figure 2. Analysis of 200 ns molecular dynamics trajectories from three simulation runs of the wild-type (chMx^{WT}) and mutant (chMx^{S631N}) chicken Mx proteins. The root mean square deviation (RMSD) of the protein backbone atoms (top), the radius of gyration (Rg) of the backbone atoms (middle), the solvent accessible surface area (SASA) at position 631 of both chMx^{WT} and chMx^{S631N} (bottom).

mutant (chMx^{S631N}) proteins. First, we analyzed the root mean square deviation (RMSD) of both models, which showed that, after 80 ns, the overall deviation was stable in the mutant (chMx^{S631N}) compared to the wild-type protein. In particular, chMx^{WT} showed large deviations in simulation runs 2 and 3 compared to chMx^{S631N} (Figures 2 and S2). The radius of gyration (Rg) showed the stable compactness of the models during simulations, with considerable variation between chMx^{WT} and chMx^{S631N}. In addition, the solvent-accessible surface area at position 631 was larger in the mutant model than in the wild-type model (Figure 2). Further, root mean square fluctuation (RMSF) analysis indicated that large fluctuations occurred at the G-domain and stalk domain in both models. However, the fluctuations at the stalk domain were similar in both models, at least in two simulation runs (Figure 3). Subsequently, to assess the variation in global motion, we performed PC analysis of the backbone atoms of the concatenated trajectory of the last 100 ns from three simulation runs of each model. The projections of PC1 and PC2, PC2 and PC3, and PC1 and PC3 are shown in Figure 4. To determine the dominant modes of motion, we generated porcupine plots for PC1, PC2, and PC3 for both wild-type and mutant chMx proteins (Figure S3).

To assess the representative structures, free energy landscape (FEL) analyses were performed using PC1 and PC2, which revealed that there may not be large transition during simulation in chMx proteins (Figure 5). We assessed representative structures from each simulation run of both systems and superimposed them onto the initial structure. This strongly suggested that the flexibility at the hinge 1 region

led to several stalk domain conformations. In particular, in chMx^{WT}, the vertical stalk domain conformation was observed in two simulation runs and a slightly inclined stalk domain conformation was observed in one simulation run, whereas in chMx^{S631N}, the inclined stalk domain conformations were observed in all of the simulation runs (Figure 5(A, B)). To determine the reason for this difference in stalk domain conformation between wild-type and mutant chMx proteins, we assessed the three representative C α atoms at residues 401, 672, and 678, at the vicinity of hinge 1, and verified the angle. We observed that the angle at the hinge 1 region was larger in chMx^{S631N} than in chMx^{WT}, indicating that hinge 1 was crucial for maintaining the inclined conformation of the stalk domain (Figure 5(C)). A recent study of the human MxB structure revealed that the dimer interface at the stalk domain was crucial for further oligomerization and for forming additional interfaces between Mx protein monomers (Alvarez et al., 2017). Hence, we hypothesize that the wild-type chMx protein, which shows a different conformation of the stalk domain compared to the mutant, may not provide the proper symmetry required for dimerization at the stalk-domain, compared to the mutant. However, further experiments and long-range simulation of Mx protein dimers are required for a better understanding of the oligomerization of the chMx protein.

Domain motion analysis

To understand domain motion during the simulations, we performed interdomain motion analysis using initial and final

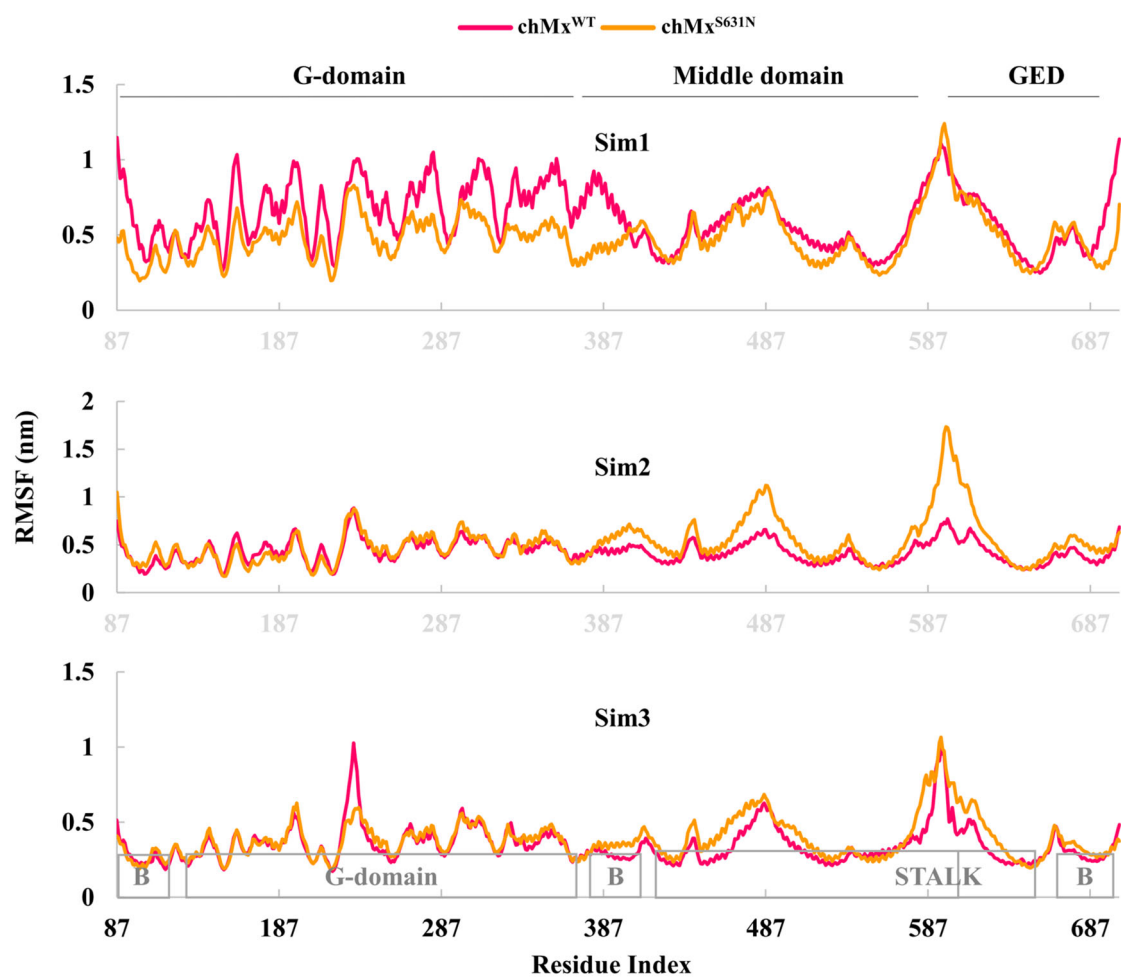


Figure 3. Root mean square fluctuations (RMSF) of the residues for the last 100 ns of the molecular dynamics trajectory (from three simulation runs) for both chMx^{WT} and $\text{chMx}^{\text{S631N}}$.

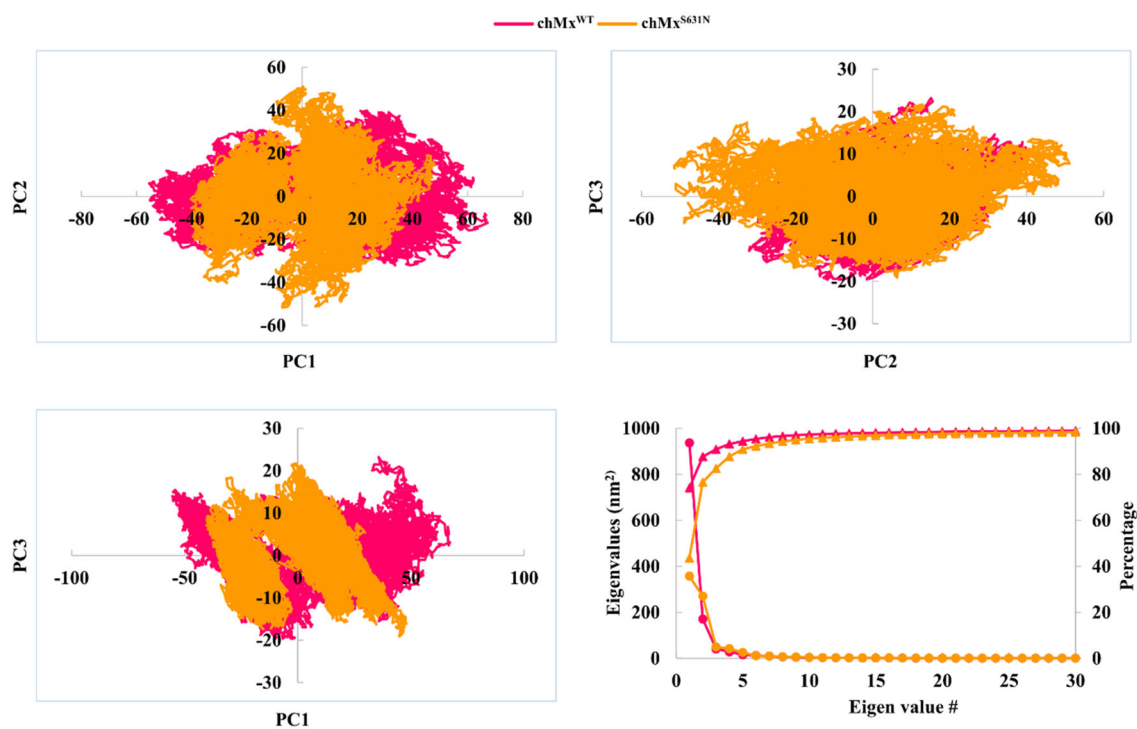


Figure 4. Projection of structural conformations extracted from the concatenated trajectory of the last 100 ns from three simulation runs onto the subspace, using principal components. Projections of the selected principal components, PC1 and PC2 (top left), PC2 and PC3 (top right), and PC1 and PC3 (bottom left) are shown. Lines with dots represent the variance of the covariance matrix, whereas lines with triangle symbols represent the cumulative percentage of variance (bottom right).

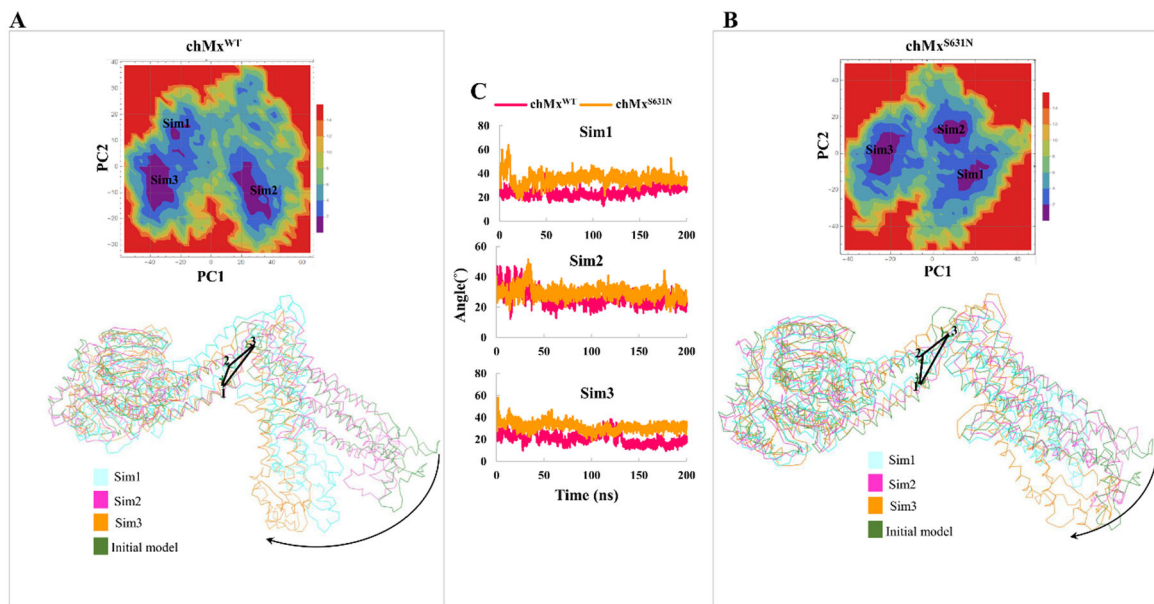


Figure 5. Structural differences between chMx^{WT} and chMx^{S631N}. (A and B) Two-dimensional plot of the free energy landscape (FEL) for the wild-type and mutant chMx proteins. Representative structures extracted from the FEL analysis were superimposed on the corresponding initial structures of chMx^{WT} and chMx^{S631N}. The conformational variation in the stalk domain of wild-type and mutant chMx is indicated with an arrow. (C) The angle between the corresponding residues (401, 672, 678) of the C α atoms along the molecular dynamics trajectory of three simulation runs for both wild-type and mutant chMx. Green stick atoms and numerical values represent the corresponding residues taken for the analysis of the hinge angle.

(representative) structures. From this analysis, we observed that chMx^{WT} possesses only one hinge region (bending residues), with only two domains as fixed and moving domains in all three simulation runs (Figure 6). The mutant, chMx^{S631N}, showed slight variation compared to chMx^{WT}, in particular simulation run 1 suggested that two interdomain hinge axes (bending residues) may be present in chMx^{S631N} through the stalk domain as the fixed domain, with two moving domains, in contrast to chMx^{WT}. However, the other two simulation runs did not show two interdomain hinge axes in chMx^{S631N}, which ultimately suggested that there may be several conformations possible at the region surrounded by mutant residue in chMx^{S631N}. Overall, a large rotation was observed in chMx^{WT}, with rotation angles of approximately 63.0°, 33.9°, and 73.5° in three simulation runs, with respect to the fixed domain (G-domain), originating from the bending residues mainly at the hinge region. In contrast to the wild-type protein, chMx^{S631N} showed two moving domains (simulation run 1) with respect to the fixed domain (stalk domain). The rotation of the first moving domain (G-domain) was approximately 51.3° and the rotation of the second moving domain was observed at the region close to the mutant residue (S631N), with a rotational angle of approximately 47.9° with respect to the fixed domain (stalk domain). In simulation runs 2 and 3, these angles were approximately 38.4° (Figure 6). This region seems to be crucial for the dimerization of the Mx protein. Moreover, the crystal and cryo-EM structures of human Mx protein have shown that the kink in the first helix of the stalk domain is crucial for dimerization. Despite four dimeric interfaces that have been identified using the cryo-EM technique in multimeric human MxB, the interface at the stalk-stalk domain is sufficient to provide the symmetrical arrangement needed for the multimerization of Mx (Alvarez et al., 2017). Hence,

since Asn is a long residue compared to Ser, we assume that the chMx S631N mutation may lead to conformational changes required to form the dimer interface, which is required for multimerization. Of note, these conformational changes were not largely observed in chMx^{WT}, suggesting an explanation for the lack of antiviral activity of chMx^{WT}, as observed in previous reports. It is also worth mentioning that human Mx proteins also contain this serine residue; however, the identity between chMx and human Mx proteins was approximately 47%, indicating that in human Mx, other residues may be responsible for providing the symmetrical environment required for dimerization.

Residue signal distribution in the wild-type and mutant chMx proteins

Further, we performed residue network analysis of the representative structures from the simulations, using the NAPS webserver. Firstly, we constructed residue networks for both chMx^{WT} and chMx^{S631N}, using a non-weighted method with a threshold of 7 Å between residue pairs of C α and C α . We then analyzed the between centrality (C_B) values of each residue, which may be crucial for signal transduction within a protein. From this analysis, using the condition of $\text{chMx}^{\text{WT}} \geq 0.2$, we observed that the most crucial residues in chMx^{WT} were located in the region of the $\alpha 2$ and $\alpha 3$ helices of the BSE and the $\alpha 1$ helix of the stalk domain, which also leads to the kink region. For chMx^{S631N}, using the condition of $\text{chMx}^{\text{S631N}} \geq 0.2$, we observed the $\alpha 2$ and $\alpha 3$ helices of the BSE and the $\alpha 2$ helix of the stalk domain, which was close to the hinge 1 region, were the most crucial residues (Figure 7). However, further experimental validation is needed for a better understanding of the impact of these crucial residues in chMx.

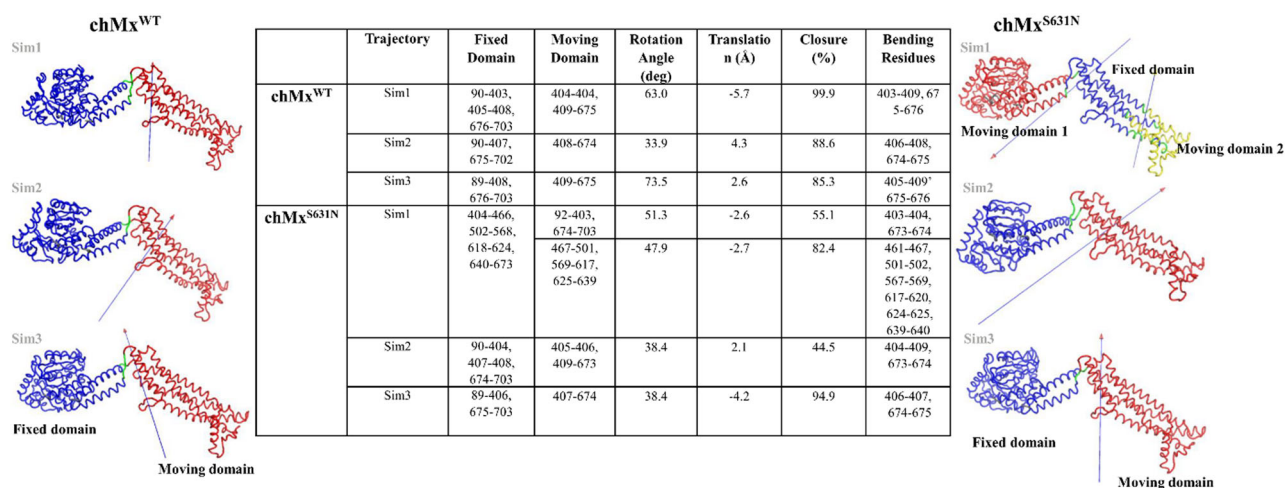


Figure 6. Interdomain analyses of the fixed and moving domains of chMx^{WT} and chMx^{S631N} are shown for both the wild-type and mutant proteins. In chMx^{WT}, the fixed domain was composed of the G-domain and a BSE (blue), and the moving domain was composed of the stalk domain (red). However, in chMx^{S631N}, the fixed domain (blue) comprised the stalk domain and moving domain 1 (red) comprised the G-domain and a BSE, while moving domain 2 (yellow) comprised the region surrounded by the mutant residue (sim1). The bending or hinge residues are shown in green. The arrows represent the rotational angle of the moving domain with respect to the fixed domain. The gray color represents the N- and C-terminal residues. The residue details of the fixed and moving domains, as well as the bending residues, are given in the table.

Discussion

Mx is crucial for antiviral activity. In mammalian species, there are two Mx proteins, MxA and MxB, that are important for antiviral activity. However, in chickens, only one Mx homolog exists. Moreover, in some instances, the chMx protein appears not to possess antiviral activity, as evidenced by several previous studies. However, in some studies, antiviral activity of chMx^{S631N} has been observed (Ko et al., 2004; Sasaki et al., 2013). In addition, it is worth noting that despite reports showing that antiviral activity is improved by the S631N polymorphism of the chMx protein, this is still debatable, since other studies have reported contradictory findings (Benfield et al., 2008). Hence in this study, we used a molecular modeling and dynamics approach to understand the impact of the S631N mutation on the structure-function relationship of the chMx protein.

At first, we generated the structural model of chMx protein using I-TASSER webserver. The main structural difference observed for chMx compared to previous crystal structures from human Mx proteins was the presence of an addition helix, which was located in a part of loop 4 in the stalk domain. This helix was recently reported in the structure of human MxB, which was solved using the cryo-EM technique (Alvarez et al., 2017). Moreover, we did not observe any hydrogen bond interactions within hinge 1, unlike in human MxA (Chen et al., 2017; Gao et al., 2011). However, hinge 2 contained a proline (Pro 334) residue, similar to human Mx proteins. The structure of chMx protein was obviously similar to that of human Mx proteins. Of note, in spite of the structural similarity to human Mx proteins, wild-type chMx protein does not show antiviral activity (Bernasconi et al., 1995). The S631N polymorphism of chMx, which is reported to be associated with anti-viral activity, is located in helix 4, which is part of the GTPase effector domain (GED, Figure 1). Initially, we assessed whether position 631 was likely to undergo posttranslational modification, such as glycosylation, which

may result in a significant impact on the overall molecular conformation of chMx protein using the glycosylation prediction program (GPP) server (Hamby & Hirst, 2008). However, we observed, that position 631 is not glycosylated according to the GPP server (data not shown).

MD trajectory analysis of RMSD, Rg and SASA (at 631 position) indicate that obvious conformational changes occurred during the simulations between wild-type and mutant chMx proteins (Figures 2 and S2). Further, RMSF suggest over all large residual flexibility in chMx^{WT} and chMx^{S631N} (Figure 3). To check the global motions, we performed PC analysis and overall, the projection of the dominant PCs indicated that the chMx^{WT} had more spreading of conformations onto the phase space, compared to the chMx^{S631N}. The small periodic jumps observed in both chMx wild-type and mutant proteins suggested that they both may undergo conformational changes during simulations. In addition, the first ten principal components of both chMx wild-type and mutant proteins showed a cumulative variance of 90% (Figure 4). Further dominant modes of motion suggest that the principal motion of PC1 for chMx^{WT} was the movement of the G-domain and stalk domain towards each other, whereas in chMx^{S631N}, the G-domain and stalk domain slightly moved towards each other. However, loop 4 in the stalk domain moved in the opposite direction compared to the wild-type protein. The second dominant motion (PC2) was the GTP-binding domain and stalk domain moving opposite to each other, whereas in chMx^{S631N}, both domains moved towards each other. The third principal motion was almost converged, with the exception of loop 4 in the stalk domain of both wild-type and mutant chMx proteins (Figure S3).

The superimposition of the representative structures constructed for each simulation run using FEL, revealed that the angle of the hinge region (hinge 1) during simulation was less in chMx^{WT} compared to chMx^{S631N} (Figure 5), which led to the stalk domain having a vertical conformation in chMx^{WT}, but an inclined conformation in chMx^{S631N},

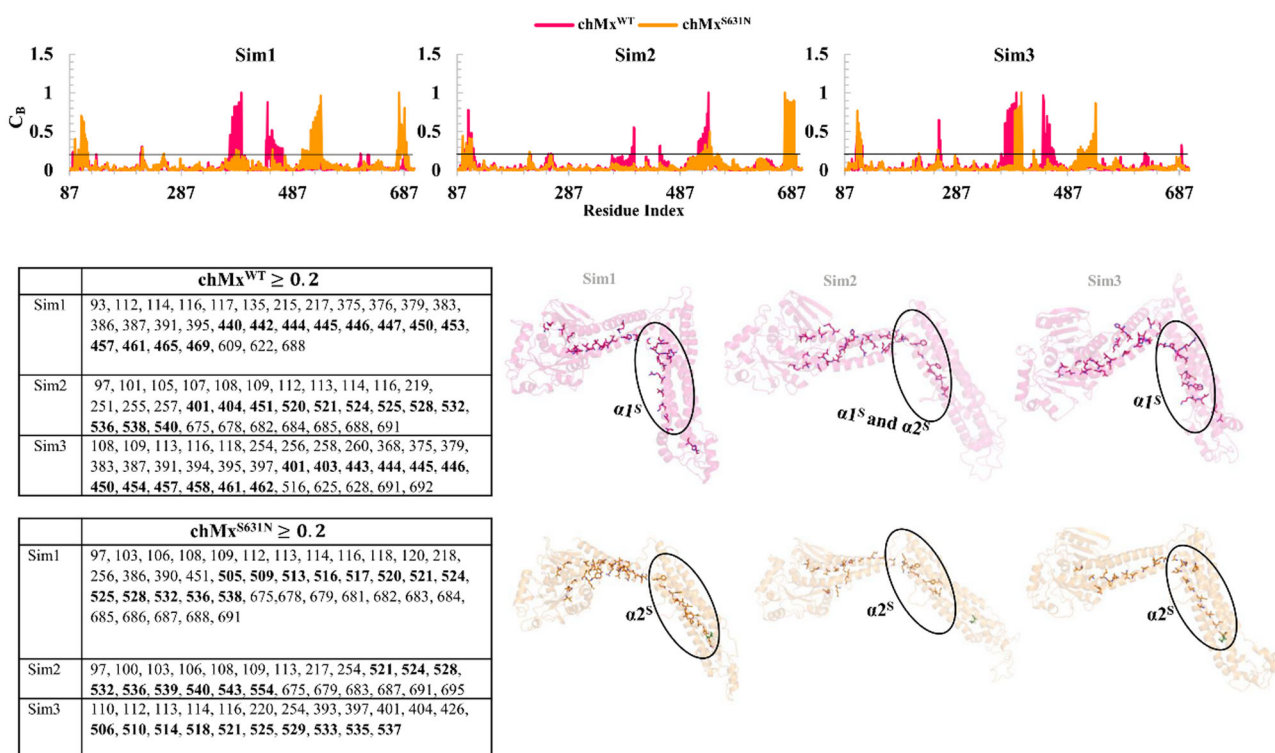


Figure 7. The betweenness centrality (C_B) of chMx^{WT} and $\text{chMx}^{\text{S631N}}$. The betweenness centrality (C_B) values were identified from residue networks constructed using the non-weighted method, with a maximum threshold of 7 Å between C α -C α pairs. The black line represents the cutoff of $C_B \geq 0.2$. The residues satisfying the condition $C_B \geq 0.2$ are shown in the table and are also mapped on the structures using a stick model. The variations in residues between chMx^{WT} and $\text{chMx}^{\text{S631N}}$ are depicted in black circles. $\alpha 1^{\text{S}}$ refers to the first helix of the stalk domain, while $\alpha 2^{\text{S}}$ refers to the second helix of the stalk domain. The mutant residue is shown in a green color with stick model.

suggesting that the inclined conformation may be crucial for the dimerization and oligomerization of Mx proteins, as observed for human Mx protein (Alvarez et al., 2017). Further, interdomain motion analysis to confirm the inclined stalk domain conformation revealed that chMx^{WT} possessed two domains (fixed domain and moving domain), whereas $\text{chMx}^{\text{S631N}}$ possessed three domains, with one fixed and two moving domains (for simulation run 1). We observed additional moving domain in the stalk domain within the region surrounded by the mutant residue, mainly in loop 4 (Figure 6). This loop is largely disordered in most of the crystal structures solved for human Mx, except in the cryo-EM structure. Cryo-EM structural analysis revealed that part of loop 4 comprised a helix, which may allow the kink region on the $\alpha 1$ helix and suggested that this kink region may be crucial for the initial dimerization of Mx proteins (Alvarez et al., 2017). We also observed slight variations at the kink region for wild-type and mutant chMx proteins (Figure S4) in the $\alpha 1$ -helix, which may allow the formation of another moving conformation in that region. From these results, we propose that the kink in the $\alpha 1$ helix may play a role in the symmetrical arrangement required for the dimerization in $\text{chMx}^{\text{S631N}}$, as evidenced by domain motion analysis for simulation run1 (Figure 6); however, we did not observe this kink in chMx^{WT} for simulation run1. Hence, the single variant, S631N, of chMx may have an impact on the structural rearrangement of the stalk domain. Previously, several computational studies have been reported that single variant of the protein may induce conformational changes which subsequently impact

on the protein function (Gosu et al., 2020; Sneha et al., 2017; Thirumal Kumar et al., 2017; Thirumal Kumar & George Priya Doss, 2017). Additionally, using residue network analysis, we identified the residue signal distribution in the wild-type and mutant chMx proteins, which also suggested variation in the major residues that contribute to intramolecular signal transduction (Figure 7).

Conclusions

In the present study, we performed multiple in-silico approaches in particular MD simulations, to shed light the conformational changes induced by S631N variant in chMx protein. Observed differences in the stalk domain conformation as well as conformational differences at the vicinity of the mutant residue in the $\text{chMx}^{\text{S631N}}$ compared to the chMx^{WT} , may be crucial for the symmetrical arrangement required for dimeric/oligomeric interface of chMx protein. Though, some experimental results suggested that S631N variant improves the antiviral activity of chMx , it is still debatable due to contradictory results have also been reported. Since, functional Mx proteins exist in dimeric/oligomeric form, long-range simulations of the dimeric/oligomeric complexes of chMx may be required to accurately determine the conformational changes crucial for antiviral activity. However, we hope that the results observed in this study provide useful information on the intrinsic dynamics and structural alterations between chMx^{WT} and $\text{chMx}^{\text{S631N}}$, which may aid in a better understanding of the antiviral activity of

chMx, that might be associated with the S631N polymorphism.

Authors contribution

Conceptualization, V.G. and K-D.S.; formal analysis, V.G. and D.S.; investigation, V.G. and D.S.; supervision, J.H. and J-D.O.; writing – original draft, V.G. and J-D.O.; writing – review & editing, K-D.S., J.H. and J-D.O.

Disclosure statement

The authors declare no conflict of interest.

Funding

This research was funded by the Next-Generation Biogreen 21 Program, Rural Development Administration, Republic of Korea, grant numbers PJ013151 and PJ01324201 and the National Research Foundation of Korea, grant number NRF-2018R1C1B6008141.

References

- Alvarez, F. J. D., He, S., Perilla, J. R., Jang, S., Schulten, K., Engelman, A. N., Scheres, S. H. W., & Zhang, P. (2017). CryoEM structure of MxB reveals a novel oligomerization interface critical for HIV restriction. *Science Advances*, 3(9), e1701264. <https://doi.org/10.1126/sciadv.1701264>
- Amadei, A., Ceruso, M. A., & Di Nola, A. (1999). On the convergence of the conformational coordinates basis set obtained by the essential dynamics analysis of proteins' molecular dynamics simulations. *Proteins: Structure, Function, and Genetics*, 36(4), 419–424. [https://doi.org/10.1002/\(SICI\)1097-0134\(19990901\)36:4<419::AID-PROT5>3.0.CO;2-U](https://doi.org/10.1002/(SICI)1097-0134(19990901)36:4<419::AID-PROT5>3.0.CO;2-U)
- Bazzigher, L., Schwarz, A., & Staeheli, P. (1993). No enhanced influenza virus resistance of murine and avian cells expressing cloned duck Mx protein. *Virology*, 195(1), 100–112. <https://doi.org/10.1006/viro.1993.1350>
- Benfield, C. T. O., Lyall, J. W., Kochs, G., & Tiley, L. S. (2008). Asparagine 631 variants of the chicken Mx protein do not inhibit influenza virus replication in primary chicken embryo fibroblasts or in vitro surrogate assays. *Journal of Virology*, 82(15), 7533–7539. <https://doi.org/10.1128/JVI.00185-08>
- Bernasconi, D., Schultz, U., & Staeheli, P. (1995). The interferon-induced Mx protein of chickens lacks antiviral activity. *Journal of Interferon & Cytokine Research*, 15(1), 47–53. <https://doi.org/10.1089/jir.1995.15.47>
- Bussi, G., Donadio, D., & Parrinello, M. (2007). Canonical sampling through velocity rescaling. *The Journal of Chemical Physics*, 126(1), 14101. <https://doi.org/10.1063/1.2408420>
- Chakrabarty, B., & Parekh, N. (2016). NAPS: Network Analysis of Protein Structures. *Nucleic Acids Research*, 44(W1), W375–W382. <https://doi.org/10.1093/nar/gkw383>
- Chen, Y., Zhang, L., Graf, L., Yu, B., Liu, Y., Kochs, G., Zhao, Y., & Gao, S. (2017). Conformational dynamics of dynamin-like MxA revealed by single-molecule FRET. *Nature Communications*, 8, 15744. <https://doi.org/10.1038/ncomms15744>
- Dillon, D., & Runstadler, J. (2010). Mx gene diversity and influenza association among five wild dabbling duck species (*Anas* spp.) in Alaska. *Infection, Genetics and Evolution*, 10(7), 1085–1093. <https://doi.org/10.1016/j.meegid.2010.07.004>
- Ewald, S. J., Kapczynski, D. R., Livant, E. J., Suarez, D. L., Ralph, J., McLeod, S., & Miller, C. (2011). Association of Mx1 Asn631 variant alleles with reductions in morbidity, early mortality, viral shedding, and cytokine responses in chickens infected with a highly pathogenic avian influenza virus. *Immunogenetics*, 63(6), 363–375. <https://doi.org/10.1007/s00251-010-0509-1>
- Gao, S., von der Malsburg, A., Dick, A., Faelber, K., Schroder, G. F., Haller, O., Kochs, G., & Daumke, O. (2011). Structure of myxovirus resistance protein a reveals intra- and intermolecular domain interactions required for the antiviral function. *Immunity*, 35(4), 514–525. <https://doi.org/10.1016/j.immuni.2011.07.012>
- Girdlestone, C., & Hayward, S. (2016). The DynDom3D webserver for the analysis of domain movements in multimeric proteins. *Journal of Computational Biology: A Journal of Computational Molecular Cell Biology*, 23(1), 21–26. <https://doi.org/10.1089/cmb.2015.0143>
- Gosu, V., Son, S., Shin, D., & Song, K.-D. (2019). Insights into the dynamic nature of the dsRNA-bound TLR3 complex. *Scientific Reports*, 9(1), 3652. <https://doi.org/10.1038/s41598-019-39984-8>
- Gosu, V., Won, K., Oh, J. D., & Shin, D. (2020). Conformational changes induced by S34Y and R98C variants in the death domain of Myd88. *Frontiers in Molecular Biosciences*, 7, 27. <https://doi.org/10.3389/fmolb.2020.00027>
- Goujon, C., Moncorge, O., Bauby, H., Doyle, T., Ward, C. C., Schaller, T., Hue, S., Barclay, W. S., Schulz, R., & Malim, M. H. (2013). Human MX2 is an interferon-induced post-entry inhibitor of HIV-1 infection. *Nature*, 502(7472), 559–562. <https://doi.org/10.1038/nature12542>
- Haller, O., & Kochs, G. (2002). Interferon-induced mx proteins: Dynamin-like GTPases with antiviral activity. *Traffic (Copenhagen, Denmark)*, 3(10), 710–717. <https://doi.org/10.1034/j.1600-0854.2002.31003.x>
- Haller, O., & Kochs, G. (2011). Human MxA protein: An interferon-induced dynamin-like GTPase with broad antiviral activity. *Journal of Interferon & Cytokine Research: The Official Journal of the International Society for Interferon and Cytokine Research*, 31(1), 79–87. <https://doi.org/10.1089/jir.2010.0076>
- Haller, O., Staeheli, P., Schwemmler, M., & Kochs, G. (2015). Mx GTPases: Dynamin-like antiviral machines of innate immunity. *Trends in Microbiology*, 23(3), 154–163. <https://doi.org/10.1016/j.tim.2014.12.003>
- Haller, O., Stertz, S., & Kochs, G. (2007). The Mx GTPase family of interferon-induced antiviral proteins. *Microbes and Infection*, 9(14–15), 1636–1643. <https://doi.org/10.1016/j.micinf.2007.09.010>
- Hamby, S. E., & Hirst, J. D. (2008). Prediction of glycosylation sites using random forests. *BMC Bioinformatics*, 9, 500. <https://doi.org/10.1186/1471-2105-9-500>
- Hayward, S. (1999). Structural principles governing domain motions in proteins. *Proteins: Structure, Function, and Genetics*, 36(4), 425–435. [https://doi.org/10.1002/\(SICI\)1097-0134\(19990901\)36:4<425::AID-PROT6>3.0.CO;2-S](https://doi.org/10.1002/(SICI)1097-0134(19990901)36:4<425::AID-PROT6>3.0.CO;2-S)
- Hayward, S., & Berendsen, H. J. (1998). Systematic analysis of domain motions in proteins from conformational change: New results on citrate synthase and T4 lysozyme. *Proteins: Structure, Function, and Genetics*, 30(2), 144–154. [https://doi.org/10.1002/\(SICI\)1097-0134\(19980201\)30:2<144::AID-PROT4>3.0.CO;2-N](https://doi.org/10.1002/(SICI)1097-0134(19980201)30:2<144::AID-PROT4>3.0.CO;2-N)
- Kane, M., Yadav, S. S., Bitzegeio, J., Kutluay, S. B., Zang, T., Wilson, S. J., Schoggins, J. W., Rice, C. M., Yamashita, M., Hatzioannou, T., & Bieniasz, P. D. (2013). MX2 is an interferon-induced inhibitor of HIV-1 infection. *Nature*, 502(7472), 563–566. <https://doi.org/10.1038/nature12653>
- Ko, J. H., Takada, A., Mitsuhashi, T., Agui, T., & Watanabe, T. (2004). Native antiviral specificity of chicken Mx protein depends on amino acid variation at position 631. *Animal Genetics*, 35(2), 119–122. <https://doi.org/10.1111/j.1365-2052.2004.01096.x>
- Lindorff-Larsen, K., Piana, S., Palmo, K., Maragakis, P., Klepeis, J. L., Dror, R. O., & Shaw, D. E. (2010). Improved side-chain torsion potentials for the Amber ff99SB protein force field. *Proteins*, 78(8), 1950–1958. <https://doi.org/10.1002/prot.22711>
- Liu, Z., Pan, Q., Ding, S., Qian, J., Xu, F., Zhou, J., Cen, S., Guo, F., & Liang, C. (2013). The interferon-inducible MxB protein inhibits HIV-1 infection. *Cell Host & Microbe*, 14(4), 398–410. <https://doi.org/10.1016/j.chom.2013.08.015>
- Muller, U., Steinhoff, U., Reis, L. F., Hemmi, S., Pavlovic, J., Zinkernagel, R. M., & Aguet, M. (1994). Functional role of type I and type II interferons in antiviral defense. *Science (New York, N.Y.)*, 264(5167), 1918–1921. <https://doi.org/10.1126/science.8009221>

- Parrinello, M., & Rahman, A. (1981). Polymorphic transitions in single crystals: A new molecular dynamics method. *Journal of Applied Physics*, 52(12), 7182–7190. <https://doi.org/10.1063/1.328693>
- Pavlovic, J., & Staeheli, P. (1991). The antiviral potentials of Mx proteins. *Journal of Interferon Research*, 11(4), 215–219. <https://doi.org/10.1089/jir.1991.11.215>
- Pronk, S., Pall, S., Schulz, R., Larsson, P., Bjelkmar, P., Apostolov, R., Shirts, M. R., Smith, J. C., Kasson, P. M., van der Spoel, D., Hess, B., & Lindahl, E. (2013). GROMACS 4.5: A high-throughput and highly parallel open source molecular simulation toolkit. *Bioinformatics (Oxford, England)*, 29(7), 845–854. <https://doi.org/10.1093/bioinformatics/btt055>
- Rothman, J. H., Raymond, C. K., Gilbert, T., O'Hara, P. J., & Stevens, T. H. (1990). A putative GTP binding protein homologous to interferon-inducible Mx proteins performs an essential function in yeast protein sorting. *Cell*, 61(6), 1063–1074. [https://doi.org/10.1016/0092-8674\(90\)90070-U](https://doi.org/10.1016/0092-8674(90)90070-U)
- Roy, A., Kucukural, A., & Zhang, Y. (2010). I-TASSER: A unified platform for automated protein structure and function prediction. *Nature Protocols*, 5(4), 725–738. <https://doi.org/10.1038/nprot.2010.5>
- Sasaki, K., Yoneda, A., Ninomiya, A., Kawahara, M., & Watanabe, T. (2013). Both antiviral activity and intracellular localization of chicken Mx protein depend on a polymorphism at amino acid position 631. *Biochemical and Biophysical Research Communications*, 430(1), 161–166. <https://doi.org/10.1016/j.bbrc.2012.11.053>
- Schusser, B., Reuter, A., von der Malsburg, A., Penski, N., Weigend, S., Kaspers, B., Staeheli, P., & Härtle, S. (2011). Mx is dispensable for interferon-mediated resistance of chicken cells against influenza A virus. *Journal of Virology*, 85(16), 8307–8315. <https://doi.org/10.1128/JVI.00535-11>
- Sneha, P., Kumar Thirumal, D., Tanwar, H., Siva, R., George Priya Doss, C., & Zayed, H. (2017). Structural analysis of G1691S variant in the human filamin B gene responsible for Larsen Syndrome: A comparative computational approach. *Journal of Cellular Biochemistry*, 118(7), 1900–1910. <https://doi.org/10.1002/jcb.25920>
- Staeheli, P. (1990). Interferon-induced proteins and the antiviral state. *Advances in Virus Research*, 38, 147–200. [https://doi.org/10.1016/S0065-3527\(08\)60862-3](https://doi.org/10.1016/S0065-3527(08)60862-3)
- Thirumal Kumar, D., & George Priya Doss, C. (2017). Role of E542 and E545 missense mutations of PIK3CA in breast cancer: A comparative computational approach. *Journal of Biomolecular Structure & Dynamics*, 35(12), 2745–2757. <https://doi.org/10.1080/07391102.2016.1231082>
- Thirumal Kumar, D., George Priya Doss, C., Sneha, P., Tayubi, I. A., Siva, R., Chakraborty, C., & Magesh, R. (2017). Influence of V54M mutation in giant muscle protein titin: A computational screening and molecular dynamics approach. *Journal of Biomolecular Structure & Dynamics*, 35(5), 917–928. <https://doi.org/10.1080/07391102.2016.1166456>
- van Aalten, D. M., Findlay, J. B., Amadei, A., & Berendsen, H. J. (1995). Essential dynamics of the cellular retinol-binding protein-evidence for ligand-induced conformational changes. *Protein Engineering*, 8(11), 1129–1135. <https://doi.org/10.1093/protein/8.11.1129>
- Van Der Spoel, D., Lindahl, E., Hess, B., Groenhof, G., Mark, A. E., & Berendsen, H. J. (2005). GROMACS: Fast, flexible, and free. *Journal of Computational Chemistry*, 26(16), 1701–1718. <https://doi.org/10.1002/jcc.20291>
- Wang, Y., Brahmakshatriya, V., Lupiani, B., Reddy, S., Okimoto, R., Li, X., Chiang, H., & Zhou, H. (2012). Associations of chicken Mx1 polymorphism with antiviral responses in avian influenza virus infected embryos and broilers. *Poultry Science*, 91(12), 3019–3024. <https://doi.org/10.3382/ps.2012-02471>
- Xu, D., & Zhang, Y. (2011). Improving the physical realism and structural accuracy of protein models by a two-step atomic-level energy minimization. *Biophysical Journal*, 101(10), 2525–2534. <https://doi.org/10.1016/j.bpj.2011.10.024>
- Yamaguchi, H., van Aalten, D. M., Pinak, M., Furukawa, A., & Osman, R. (1998). Essential dynamics of DNA containing a cis.syn cyclobutane thymine dimer lesion. *Nucleic Acids Research*, 26(8), 1939–1946. <https://doi.org/10.1093/nar/26.8.1939>
- Yang, J., Yan, R., Roy, A., Xu, D., Poisson, J., & Zhang, Y. (2015). The I-TASSER Suite: Protein structure and function prediction. *Nature Methods*, 12(1), 7–8. <https://doi.org/10.1038/nmeth.3213>
- Zürcher, T., Pavlovic, J., & Staeheli, P. (1992). Nuclear localization of mouse Mx1 protein is necessary for inhibition of influenza virus. *Journal of Virology*, 66(8), 5059–5066. <https://doi.org/10.1128/JVI.66.8.5059-5066.1992>